Interactive Modeling and Evaluation of Tumor Growth

Jacob Scharcanski,[1] Luciano Silva da Silva,[1] David Koff,[2] and Alexander Wong[3]

This paper addresses the need to quantify tumor growth and detect changes as this information is relevant to manage the patient treatment and to aid biotechnological efforts to cure cancer (Silva et al. 2008). An interactive tumor segmentation technique is used to recover the shape and size of tumors without imposing shape constraints. This segmentation algorithm provides good convergence, is robust to the initialization conditions, and requires simple and intuitive user interactions. A parametric approach to model tumor growth analytically is proposed in this paper. The preliminary experimental results are encouraging. The segmentation method is shown to be robust and simple to use, even in situations where the tumor boundary definition is challenging. Also, the experiments indicate that the proposed model potentially can be used to extrapolate the available data and help predict the tumor size (assuming unconstrained growth). Additionally, the proposed method potentially can provide a quantitative reference to compare the tumor shrinkage rate in cancer treatments.

KEY WORDS: Computed tomography (CT), image segmentation, active contours, lung cancer, computer-assisted diagnosis, chest radiographs, computer analysis, computer vision, diagnostic imaging, digital image processing, cancer detection

INTRODUCTION

T he quantitative measurement of tumor growth provides relevant information for the management of the patient treatment and to aid biotechnological efforts to cure cancer through early assessment of growth pattern and response to chemotherapy.[1] One of the difficulties faced in quantifying tumors is that the process is specific to the individual event and to the particular organ. Another important quantification difficulty is the dose–response relationships existing for various therapeutic agents. Mathematical models for tumor growth have been studied for over a century, and at this stage, there is a lack of uniform opinion in the literature regarding the appropriate model for the growth rate of human cancers.

The necessity for intensive follow-up of patients in the primary stage of the cancer has been debated. When growth rate is estimated from measurements, inaccuracies in measurement become more important. Therefore, measurement uncertainties can be reduced by adopting image processing methods specific for image segmentation and using image comparison approaches that do not deform the original data while being robust to noise and the inherent variability of computed tomography (CT) image properties. This work presents a method to build data-driven tumor growth models on sample cases of lung cancer using as inputs the changes in size measured at different stages of tumor development. At each stage of tumor development, the tumor size is measured by an interactive segmentation algorithm.

Many methods for tumor segmentation and registration rely on deformation models.[2,3] In the work of Clatz et al.,[4] the patient image is registered with an anatomical atlas, and the finite element method is used to simulate tumor growth. Zacharaki

[1]From the Instituto de Informática, Universidade Federal do Rio Grande do Sul, Caixa Postal 15064, 91501-970, Porto Alegre, RS, Brazil.

[2]From the Department of Radiology, McMaster University, Hamilton, ON, L8N 3Z5, Canada.

[3]From the Systems Design Engineering, University of Waterloo, Waterloo, N2L 3G1, Canada.

Correspondence to: Jacob Scharcanski, Instituto de Informática, Universidade Federal do Rio Grande do Sul, Caixa Postal 15064, 91501-970, Porto Alegre, RS, Brazil; tel: +55-51-33087128; fax: +55-51-33087308; e-mail: jacobs@ inf.ufrgs.br

et al.[5] applied a multimodal registration and fusion approach to simulate 3D tumor growth, but results are reported only for registered images with no significant temporal gap. A hybrid approach for semi-automated measurement of lung tumor thickness was proposed by Armato et al.[6] In their approach, the user indicates initial endpoints along the outer tumor margin; these user-defined endpoints are refined by further processing, and an estimate of the maximum tumor diameter is obtained. However, the maximum tumor diameter is a limited measure to quantify the tumor growth, since the shape of a tumor can be complex and contain concavities. Thresholding techniques and morphological operators have been used to segment lung tumors,[7] leading to measures such as the greatest diameter (1D), the product of greatest diameter and greatest perpendicular diameter (2D), and volumetric measures (3D). These measures have been proposed to analyze CT scans obtained before and after patient treatment, and the detected measurement changes were compared with ground truth data. The comparison results indicate that 2D and 3D measurements are preferable compared to 1D measurements; however, Zhao et al.[7] observed that thin-section CT series are important to guarantee reliable volume measurements. Additionally, the segmentation algorithm employed by them may require manual delimitation of the region of interest, especially when the region of interest and the tumor present similar attenuations (e.g., when a lesion is attached to the mediastinum or to the combined right diaphragm and liver). Haney et al.[8] evaluated methods for tumor growth rate estimation and compared two 3D image analysis algorithms, namely, nearest-neighbor tissue segmentation and surface modeling, both applied to magnetic resonance images of patients with gliobastoma multiform. In their comparison of the tumor growth rates computed using both segmentation methods with ground truth data, the nearest-neighbor segmentation algorithm presented better results. Nevertheless, this method requires complex user interactions, since a high number of tags (160) has to be selected by the user.

Our main goals in this work are: (a) to quantify tumor growth and changes in tumor size; and (b) to build an analytic tumor growth model as a reference to assess the tumor development. In the present work, a method for interactive segmentation and modeling of the development of lung tumors on CT scans is presented. The only interaction needed is the selection, by the specialist, of a point within the lung tumor in the more central slice of a CT scan image stack. The tumor outline is then detected by an active-contour method (i.e., snake) proposed by Xu and Prince,[9] which has two important properties for our purposes: robustness to initialization and convergence to concave boundaries. The segmentation results is used to recover automatic measurements, such as tumor shape changes and growth rate. Based on measurements on the segmentation results, an analytic tumor growth model is built. This model can be used in applications such as tumor growth prognosis or for evaluating quantitatively the effectiveness of a cancer treatment, comparing the measured tumor shrinkage rate with the prediction generated by the model.

This paper is organized as follows. Initially, the interactive tumor segmentation and area measurement is outlined in "Tumor Segmentation Using Active Contours". The tumor growth model is presented in "Modeling Unconstrained Tumor Growth" and our experimental results in "Experimental Results". Finally, the conclusions are presented in "Conclusions."

TUMOR SEGMENTATION USING ACTIVE CONTOURS

Active contours, or snakes, are curves defined in the image domain used to locate object boundaries.[10] These curves can move under the influence of internal forces and external forces. External forces are based on image measurements and are designed to move points of the curve towards the desired features (usually edges). Internal forces are related to properties of the curve itself and are designed to hold the curve together (i.e., elasticity forces) and to keep it from bending too much (i.e., bending forces).

Usually, a snake is a curve that evolves by minimizing an energy functional E in the image spatial domain:

$$E = \int_0^1 \frac{1}{2} \left(\alpha |\mathbf{x}'(s)|^2 + \beta |\mathbf{x}''(s)|^2 \right) + E_{ext}(\mathbf{x}(s))ds,$$

(1)

where, $\mathbf{x}(s) = [x(s), \ y(s)]$, $s \in [0,1]$, represent a spatial location in the curve, and α and β are weighting parameters that control the snake tension

and rigidity, respectively. The first and second derivatives of $\mathbf{x}(s)$ in relation to s are $\mathbf{x}'$ and $\mathbf{x}''$. The energy function E_{ext} represents the external forces derived from image measurements and has smaller values in image locations where the features of interest occur.

In lung tumor segmentation, the image gradient is a feature of interest, since the margins of lung tumors often correspond to sharp edges in CT images. Then, the external force function can be defined as the negative of the local image gradient $\nabla f(x, y)$:

$$E_{ext}(x,y) = -|\nabla f(x,y)|^2,$$

and a snake that minimizes E must satisfy the Euler equation:

$$\alpha\mathbf{x}''(s) - \beta\mathbf{x}'''(s) - \nabla E_{ext} = 0. \quad (2)$$

Considering that $\mathbf{x}$ is a function of time t, the partial derivative of $\mathbf{x}$ with respect to t is given by the left hand side of Eq. 2:[9]

$$\mathbf{x}_t(s,t) = \alpha\mathbf{x}''(s,t) - \beta\mathbf{x}'''(s,t) - \nabla E_{ext}. \quad (3)$$

A solution for the snake $\mathbf{x}(s,t)$ is found when the term $\mathbf{x}_t(s,t)$ reaches steady state. This result implies that the external force is proportional to the intensity of edges and only acts near the edge locations. However, despite its simplicity, this formulation has two important drawbacks: (1) makes it difficult to approximate concave regions,[11] posing difficulties for detecting the boundaries of lung tumors if they present irregular shapes, which often is the case in such tumors; (2) the initial values of $\mathbf{x}_t(s,t)$ (i.e., $\mathbf{x}_0(s,t)$) must be very close to the actual tumor margins (i.e., the tumor boundaries), and this initialization scheme may be impractical. Therefore, a different approach should be used.

Xu et al.[9] proposed a new external function, called Gradient Vector Flow, that overcomes the above mentioned problems by assuming that, in the absence of other local evidences in the image, local information vary smoothly in all directions. Therefore, the information available near the image edges can propagate across adjacent homogeneous regions, allowing to develop the snake convergence process away from the image edges (if the image boundaries are avoided). This is achieved by defining a vector field $\mathbf{v}(x,y)=(u(x, y), v(x, y))$ that minimizes the energy function:

$$\varepsilon = \iint \mu\left(u_x^2 + u_y^2 + v_x^2 + v_y^2\right) + |\nabla f|^2|\mathbf{v} - \nabla f|^2 dxdy,$$

for the sake of notation simplicity, the coordinates (x,y) have been omitted, and $f \equiv f(x, y)$. Note that when $|\nabla f|$ is small, the energy is dominated by the partial derivatives of the vector field, and when $|\nabla f|$ is large, the energy is dominated by the second term and is minimized by making $\mathbf{v} = \nabla f$. The parameter μ is a tradeoff between the first term and the second term and is set according to the noise level in the image (we used $\mu = 0.05$ in all our experiments).

As demonstrated by Xu et al., the gradient vector flow field $\mathbf{v}(x,y)$ can be found by solving the following Euler equations:

$$\mu\nabla^2 u - (u - f_x)\left(f_x^2 + f_y^2\right) = 0$$
$$\mu\nabla^2 v - (v - f_y)\left(f_x^2 + f_y^2\right) = 0,$$

where, ∇^2 is the Laplacian operator.

After $\mathbf{v}(x,y)$ is computed, it replaces the negative of the external force ($-\nabla E_{ext}$) in Eq. 3, and the value of $\mathbf{x}_t(s,t)$ is obtained at time t:

$$\mathbf{x}_t(s,t) = \alpha\mathbf{x}''(s,t) - \beta\mathbf{x}'''(s,t) + v. \quad (4)$$

In all our experiments, we used $\alpha=5$ and $\beta=50$.

Figure 1 shows an example of gradient vector flow field. Figure 1a displays the tumor region cropped from an original CT image, and Figure 1b shows the corresponding negative of the gradient ($-|\nabla f(x, y)|^2$), which is obtained with the Prewitt operator.[12] The gradient vector flow field obtained is showed in Figure 1c, and a zoom of the same flow is displayed in Figure 1d.

The tumor segmentation process is semi-automatic, in the sense that it uses a simple user interaction. All the user have to do is to select any point inside the tumor region. Once this internal point is selected, the curve $\mathbf{x}_0(s,t)$ (Eq. 4) is initialized with a small circle (radius=12 pixels), and the selected point is the circle center, as showed in Figure 2a. The iterative active contour approximation is then performed (Fig. 2b, c) until convergence ($|x_{t+1}(s, t+1) - x_t(s, t)|^2 \leq 0.5$ for all $s \in [0,1]$), as shown in Figure 2d.
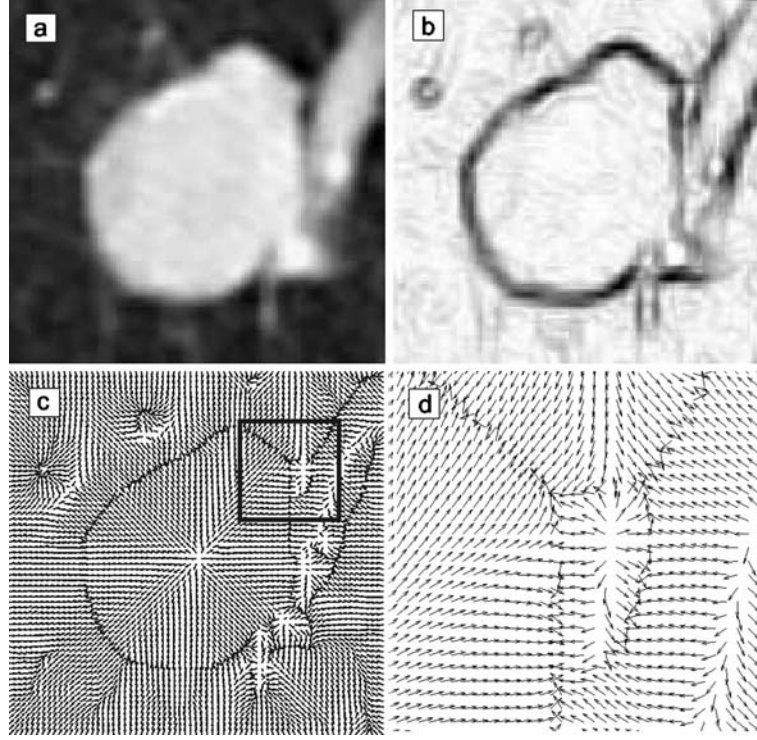
Fig 1. Example of gradient vector flow field: a original image; b negative of the gradient; c gradient vector flow field down sampled by a factor of 0.5; and d zoom of area of the flow field indicated by the rectangle in c.

The tumor perimeter in a given CT slice is estimated based on the calculated active contour boundaries, after convergence, and the tumor area is estimated based on the number of pixels within the area delimited by active contour boundaries.

As mentioned before, this active contour method is able to converge even for irregularly shaped tumors, as illustrated in Figure 3. Besides, the active contour boundaries tend to be robust to the selection of initial points within the tumor (see "Experimental Results").

MODELING UNCONSTRAINED TUMOR GROWTH

In this section, an analytical model for tumor temporal evolution is discussed. This model can be used to predict tumor growth (i.e., prognosis for a given number of time units, e.g., days), or, in the opposite way, to predict tumor shrinkage, which can be an interesting application.

Assuming that tumors as masses are approximately dense and that each tumor cell generates continuously new tumorous cells (i.e., the tumor growth is not constrained), in a time increment dt, the number of tumorous cells N_c grows by:

$$N_c(t + dt) - N_c(t) \approx \frac{dN_c}{dt} dt + \dots, \quad (5)$$

where the right hand side comes from a Taylor series expansion. Consequently, based on these assumptions, the initial number of cells $N_c(t)$ grows by a rate r in time increment dt:

$$\frac{dN_c}{dt} dt = rN_c(t)dt. \quad (6)$$

Dividing Eq. 6 by dt, an ordinary differential equation is obtained:

$$\frac{dN_c}{dt} = rN_c(t), \quad (7)$$

which has the following solution:

$$N_c(t + dt) = e^{rdt}N_c(t). \quad (8)$$

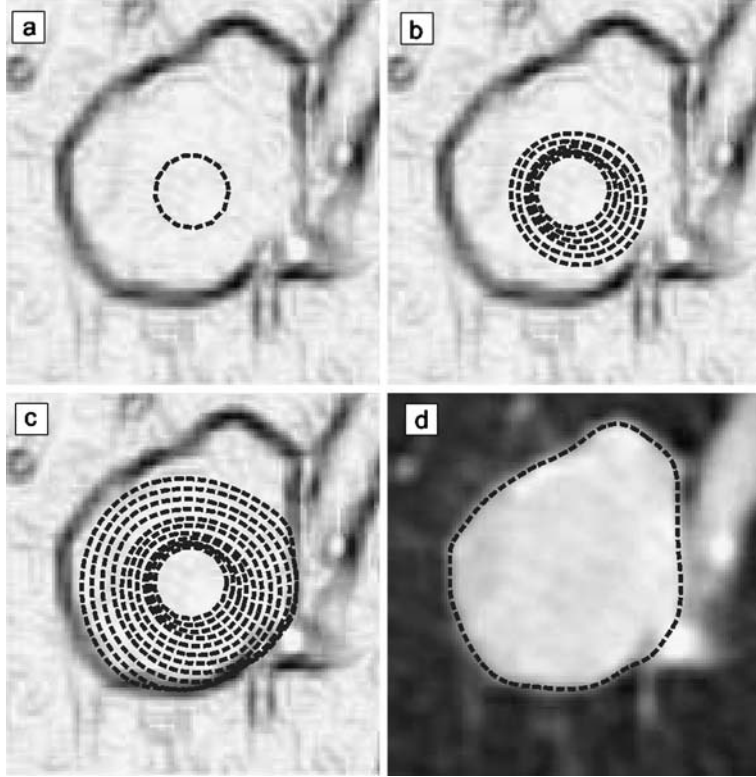Now, considering that each tumor cell occupies A_c area units in a computerized tomography slice,

Fig 2. Active contour convergence: a curve initialization, based on the seed point; b corresponding curve after 25 iterations—one curve is shown for every five iterations; c corresponding curve after 50 iterations; and d final curve (after convergence).

N_c cells occupy $N_c A_c$ area units, and the corresponding area grows proportionally to the tumor growth rate r. Therefore, assuming unconstrained tumor growth, the following exponential tumor area growth model is justifiable:

$$A_c N_c(t + dt) = e^{rdt} A_c N_c(t), \qquad (9)$$

or yet,

$$A(t + dt) = e^{rdt} A(t), \qquad (10)$$

where, $A(t)$ is the tumor area measured at time t, and $A(t+dt)$ is the area the tumor shall occupy at time $t+dt$.

In order to fit the generic exponential model (see Eq. 11) to a set of tumor areas measured at discrete times, namely $A_{t_1}, A_{t_2}, \ldots, A_{t_n} \equiv \{A_n\}$, the exponential model can be linearized, and then least-squares techniques can be used to find the model parameters. Without loss of generality, we can write Eq. 11 as:

$$A(t) = e^{rt} A(0) = e^{rt} a. \qquad (11)$$

Taking the logarithm of both sides, we obtain:

$$lnA(t) = \ln a + rt, \qquad (12)$$

or yet,

$$y = c_0 + c_1 t, \qquad (13)$$

where, $y = \ln A(t)$, $c_0 = \ln a$, and $c_1 = r$. Now, the problem of fitting the exponential model to the set
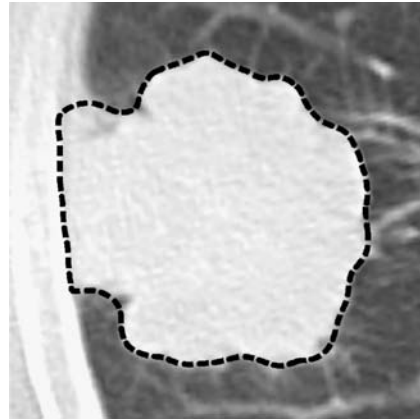

Fig 3. Complex-shaped tumor with corresponding snake overlayed.

$\{A_n\}$, has been reduced to the simpler problem of fitting a linear model (see Eq. 13) to $\ln\{A_n\}$, using least-squares techniques.

In order to calculate the least squared error estimates for the linear model parameters, let the model errors e_i be:[13]

$$
\begin{aligned}
e_1 &= A(t_1) - c_0 - c_1 t_1, \\
e_2 &= A(t_2) - c_0 - c_1 t_2, \\
&\ldots \\
e_n &= A(t_n) - c_0 - c_1 t_n.
\end{aligned}
\tag{14}
$$

Let the sum of squared errors be ε:

$$
\varepsilon = \sum_{i=1}^{n} e_i^2 = \sum_{i=1}^{n} (A(t_i) - c_0 - c_1 t_i)^2. \tag{15}
$$

Now, the least-squares criterion is used to choose c_0 and c_1 while minimizing the fitting error ε. Setting the derivatives to zero, we obtain:

$$
\frac{\partial \varepsilon}{\partial c_0} = -2 \sum_{i=1}^{n} (A(t_i) - c_0 - c_1 t_i) = 0, \tag{16}
$$

and,

$$
\sum_{i=1}^{n} A(t_i) = n c_0 + c_1 \sum_{i=1}^{n} t_i. \tag{17}
$$

Also, the derivative of ε with respect to c_1 gives:

$$
\frac{\partial \varepsilon}{\partial c_1} = -2 t_i \sum_{i=1}^{n} (A(t_i) - c_0 - c_1 t_i) = 0, \tag{18}
$$

and

$$
\sum_{i=1}^{n} t_i A(t_i) = c_0 \sum_{t_i}^{n} t_i + c_1 \sum_{i=1}^{n} t_i^2. \tag{19}
$$

Observing that Eqs. 17 and 19 are two independent equations with two unknowns c_0 and c_1, these equations can be written in matrix form as:

$$
\begin{bmatrix} n & \sum_{i=1}^{n} t_i \\ \sum_{i=1}^{n} t_i & \sum_{i=1}^{n} t_i^2 \end{bmatrix} \begin{bmatrix} c_0 \\ c_1 \end{bmatrix} = \begin{bmatrix} \sum_{i=1}^{n} A(t_i) \\ \sum_{i=1}^{n} t_i A(t_i) \end{bmatrix}. \tag{20}
$$

By solving Eq. 20 for c_0 and c_1, we obtain the parameters a and r of the exponential growth model such that the squared adjustment error is minimized:

$$
\begin{aligned}
a &= e^{c_0}, \\
r &= c_1.
\end{aligned}
\tag{21}
$$

Therefore, the exponential growth model shown in Eq. 11 becomes:

$$
A(t) = e^{c_1 t + c_0}. \tag{22}
$$

EXPERIMENTAL RESULTS

The segmentation method and proposed modeling approach have been tested using MATLAB 7.0 and IBM-PC-based computers, with 2 GB of RAM, and clock of 2 GHz. Considering that our goal in this paper is to propose an interactive tool for assessing tumor growth patterns, a prototype was assembled as a proof of concept, and its performance is illustrated using sets of thorax CT scans. As a next step in our research, we plan to investigate the growth patterns of specific types of tumors in clinical trials, and the results shall be reported separately.

In order to segment the tumor boundaries and estimate the tumor size, we use the methodology known as Response Evaluation Criteria in Solid Tumours (RECIST).[14] According to RECIST, the longest diameter of the target lesion should be obtained in the axial plane only. Therefore, we illustrate our tumor segmentation based on the slice showing the largest tumor diameter.

In order to assess the tumor growth potential and evolution, several studies on a period of time are compared. The radiologist must make sure that the lesion he/she points is the same on different studies, as often those patients have multiple metastases. Since the radiologist may wish to compare several studies, he/she often has to point the same tumor in different studies; therefore, the tumor segmentation process must be repeatable (i.e., even if the radiologist points the tumor at a different pixel, the computation should converge to similar results). As mentioned before, the active contour method based on gradient vector flow tends to be robust to initialization (i.e., to the initial point selected inside the tumor to start the segmentation process). To measure the sensitivity of the proposed approach with respect to its initialization, we compared several initializations
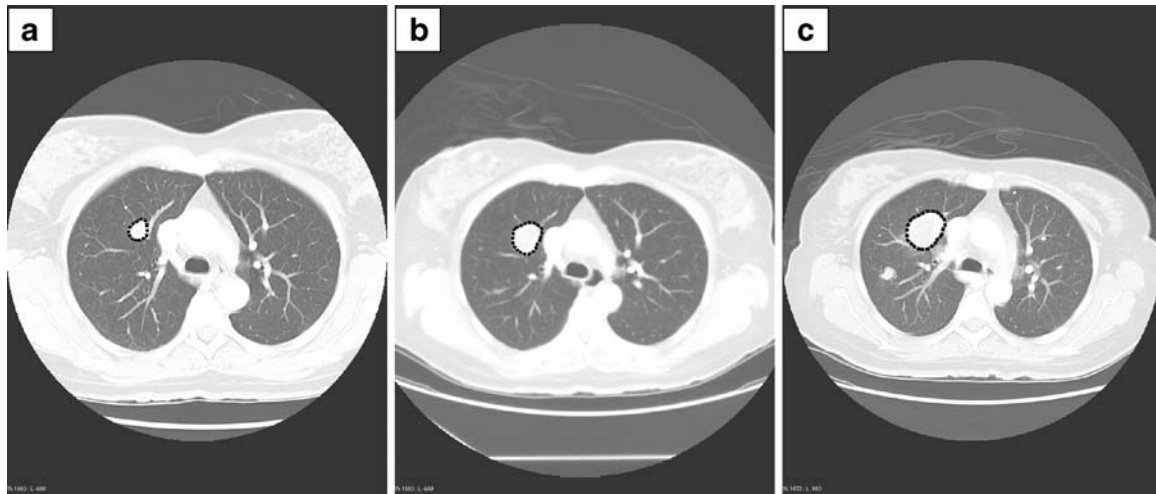
Fig 4. Segmented tumor boundaries (*dotted curve*) illustrated for the central slice of case 1 and tumor growth: a initial observation (June 04, 2007); b October 04, 2007; c November 11, 2007.

in the segmentation of the same tumor and observed the resulting segmentation maps (i.e., given an image, we marked different initial points inside a tumor region and observed the segmentation results obtained for that tumor). Experimentally, we observed that the segmentation maps obtained differ in at most 7 pixels (i.e., in the worst case). The tumor regions tested ranged from approximately 5,000 to 30,000 pixels. Therefore, provided different initializations for the same tumor segmentation process, a variation of less than 0.2% was experimentally observed. Recall that the tumor segmentation process is semi-automatic, and the user simply needs to select any point inside the tumor region.

The proposed method can be specially efficient for comparing tumors at distinct development stages. Figures 4 and 5 show examples of the final tumor segmentation, each resulting from the evolution of an active contours from a point selected in the interior of the tumor region (dotted curves). These figures show the segmentations of the same tumor developing in time, as they appear in subsequent CT scans.

The temporal evolution of tumors (as appearing in subsequent CT scans), the exponential model fit to the measurements, and the tumor size prognoses after 90 days of unconstrained growth are shown in Figures 6 and 7 for cases 1 and 2, respectively. The numerical results are reported in Table 1. It should be observed that tumors present growth

modes, and these growth modes can change with the tumor evolution, causing changes in angles and eigenvalue ratios of the largest eigenvectors. Figure 8a–c illustrates segmented tumor boundaries (dotted curves) in subsequent CT scans, and Figure 8d illustrates the evolution of a tumor with ellipse approximations (continuous curves), as well as the 90 days prognosis (dotted curve), all generated using the exponential model.

Measuring the tumor evolution in subsequent CT scans is not trivial, since implicit measurement inaccuracies exist. Often, the same tumor sections are not captured in corresponding tomographic slices of subsequent CT scans; consequently, comparative area (or volume) measurements are just approximations. In order to compare tumor sections in subsequent scans, nonlinear image registration techniques have been employed (see details in the study of Wong and Bishop[15]). However, even state-of-the-art nonlinear registration techniques can introduce tumor shape size deformations. For example, using the nonlinear registration method described in Wong and Bishop[15] in case 2, the tumor areas measured in slices 1, 2, and 3 are 10381, 12093, and 29494, respectively, indicating growth rates of 16.49% and 143.89%, for slices 2/1 and 3/2, respectively. Nevertheless, applying only linear transforms to the images (avoiding tumor shape and size deformations, which is our proposed approach), the measured tumor areas in slices 1, 2, and 3 are 10308, 12088, and 29429, respectively,

indicating growth rates of 17.2% and 143.46% for slices 2/1 and 3/2, respectively. Figure 9a–d illustrates the area growth in case 2, using the linear and the nonlinear registration approaches. The relative tumor sizes and shape differences are noticeable in the comparison of panels a and c, and panels b and d of Figure 9.

Figure 10 illustrates our analytic tumor growth model applied to case 3, where it provides a reference to assess tumor shrinkage (as a tumor response to treatments). The tumor area shrinkage based on the different observations, approximated by ellipses, and the 90 days prognosis obtained using the exponential model are shown in Figure 10a. The exponential model fit to the measured tumor areas and the 90 days prognosis based on the tumor shrinkage rate according to the exponential model are shown in Figure 10b.

Discussion

Tumors do not share the same growth pattern, according to the nature of the disease, and it is important to assess the growth trend. Most of the
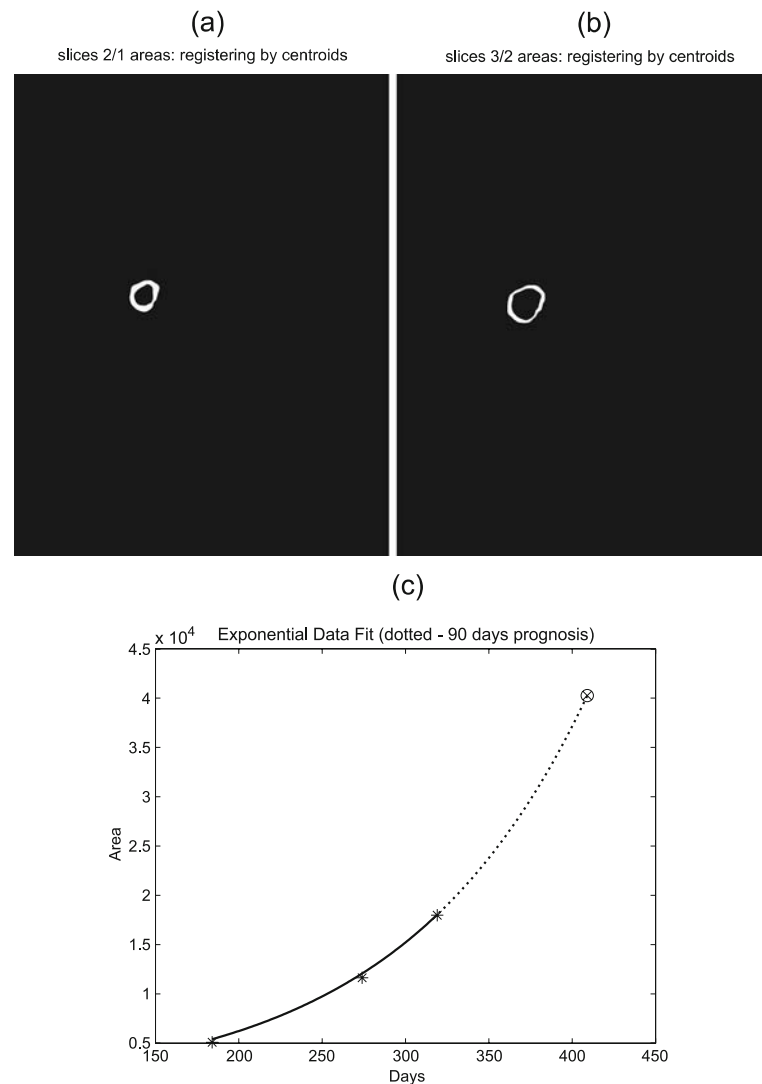
(a)

slices 2/1 areas: registering by centroids

(b)

slices 3/2 areas: registering by centroids

(c)

Fig 5. Segmented tumor boundaries (*dotted curve*) illustrated for the central slice of case 2 and tumor growth: a initial observation (April 09, 2007); b August 30, 2007; c December 27, 2007.
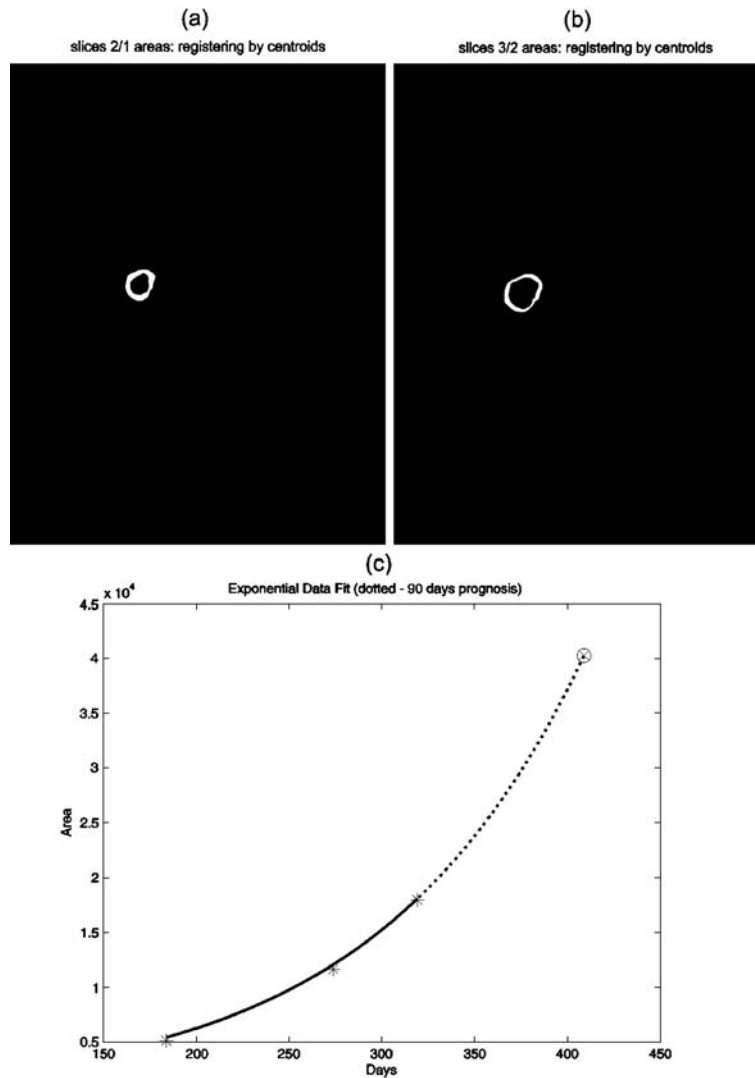
Fig 6. Measured tumor area growth based on the central slice (case 1). Tumors are registered using linear transformations (centroid adjustment): a area growth from June 04, 2007 to October 04, 2007; b area growth from October 04, 2007 to November 11, 2007; c exponential model fit to the measured tumor areas (*solid line*), and the 90 days prognosis considering unconstrained tumor growth (*dotted line*).

time, tumor measurements are taken in two or three directions, taking usually the largest diameters. Having the previous studies is important as the reader will try to reproduce the measurements at the same level of the CT scan, but it may be difficult if the tumor shape has changed. There are inter-observer differences; sometimes in the way they put the calipers, some will always take orthogonal measurements, with lines parallel to the axis of the CT slice, while others will look for the largest dimensions. Some will measure from

inside border to inside border, others to outside limits. Some may even include the peritumoral infiltration, which makes the comparison even more complex. Therefore, a mathematical representation is needed to ensure better reproducibility and more scientific assessment of the tumor potential. Our main goals of this work are: (a) to reduce the inter-observer variability in tumor size measurements and (b) to build an analytic tumor growth model as a reference to assess the tumor development. The expected benefits are: (a) assess

(a)
slices 2/1 areas: registering by centroids

(b)
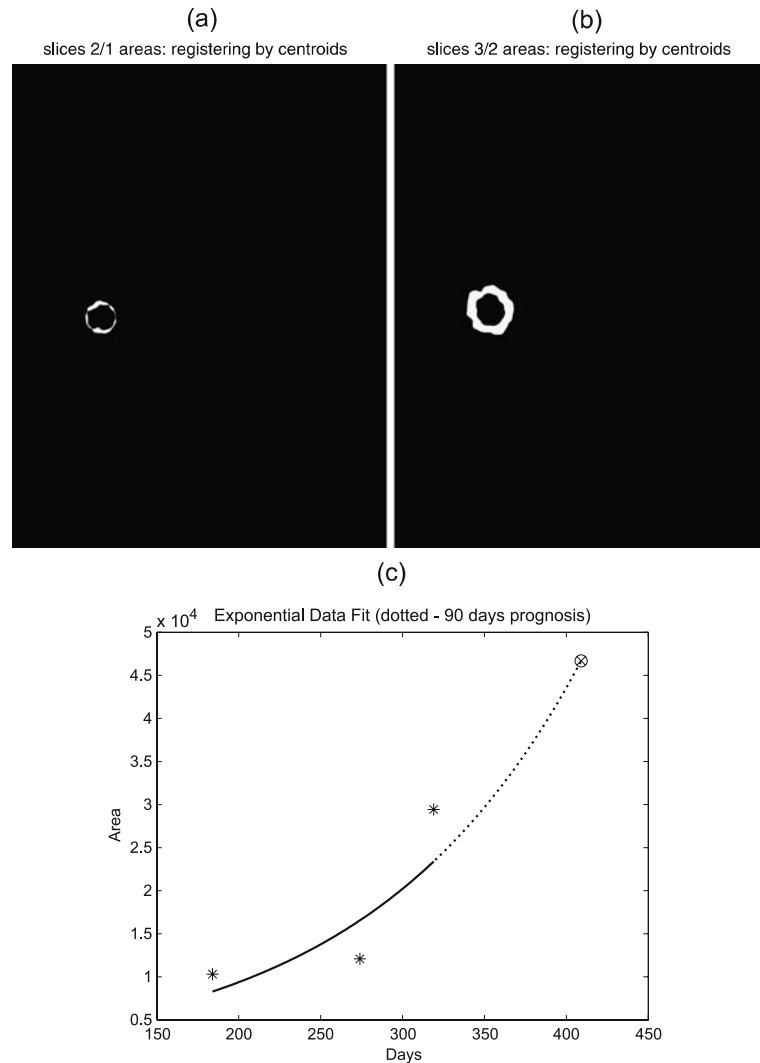slices 3/2 areas: registering by centroids

(c)

Fig 7. Measured tumor area growth based on the central slice (case 2). Tumors are registered using linear transformations (centroid adjustment): a area growth from April 09, 2007 to August 30, 2007; b area growth from August 30, 2007 to December 27, 2007; c exponential model fit to the measured tumor areas (*solid line*), and the 90 days prognosis considering unconstrained tumor growth (*dotted line*).

the tumor aggressiveness in evaluating the speed at which the tumor is progressing; (b) assess the response of the tumor to treatments and the rate at which it decreases in size and also to extract reproducible values over the period of time which can be compared to the evolution of the same type of tumor with similar treatment; (c) create a growth pattern, and this is the most innovative part of our study, as the shape of the tumor is usually overlooked. This will allow us to predict the harmful potential to neighboring organs and anticipate more accurately the complications and maybe the need

for more aggressive treatment orientation. Mainly, it will be interesting to assess potential invasion or rupture of adjacent vessels and extract trends as all tumors may not have the same pattern.

The proposed tumor segmentation method potentially can be used to estimate the size of tumors based on the number of pixels in the segmented area[14] (since the area corresponding to its pixel is known in a calibrated CT equipment). This segmentation method has been designed to be robust to initialization, flexible to handle irregularly shaped tumors, simple to use, and to reduce

Table 1. Numerical Experimental Results

Measured features	1st observation	2nd observation	3rd observation	1st/2nd observation	2nd/3rd observation
Measurements in case 1					
Perimeter (pixels)	234	357	439		
Area (pixels)	5,103	11,637	17,984		
Angle of largest eigenvector (degrees)	−144.55	−145.70	47.05		
Eigenvectors ratio (largest/smallest)	1.45	1.31	1.41		
Perimeter growth rate (pixels)				52.56	22.97
Area growth rate (pixels)				128.04	54,54
Measurements in case 2					
Perimeter (pixels)	347	370	612		
Area (pixels)	10,308	12,088	29,429		
Angle of largest eigenvector (degrees)	73.94	164.66	140.58		
Eigenvectors ratio (largest/smallest)	1.50	1.19	1.18		
Perimeter growth rate (pixels)				6.63	65.41
Area growth rate (pixels)				17.27	143.46

the inter-observer variability in measurements; and these features were verified experimentally. Also, it shall be observed that nonlinear image registration techniques tend to produce tumor shape distortions, which interferes with the size measurements (this often occurs when comparing tumor shapes in two or three dimensions). Therefore, we avoid shape distortions using linear methods to compare area (or volume) measurements.

The proposed analytic tumor growth model provides a reference to assess tumor growth or tumor shrinkage, measure the response of the
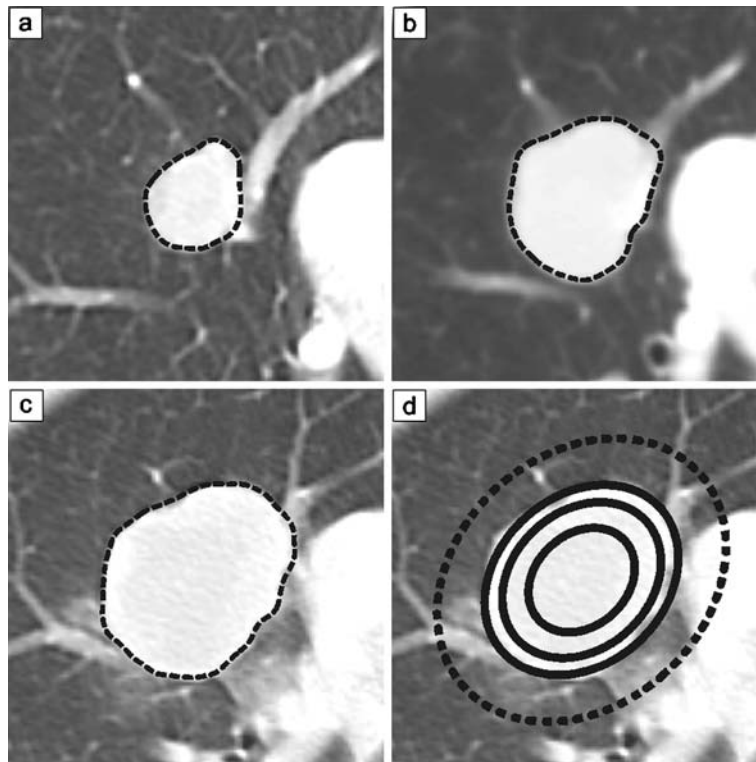

Fig 8. Segmented tumor boundaries (*dotted line*) illustrated for the central slice of case 1, and tumor growth: a initial observation (June 04, 2007); b October 04, 2007; c November 11, 2007; d tumor development based on the different observations, approximated by *solid line ellipses* and the 90 days prognosis obtained using the exponential model (*dotted line ellipsis*).

(a)

slices 2/1 areas: registering by centroids

(b)

slices 3/2 areas: registering by centroids

(c)

slices 2/1 areas: using non-linear registration

(d)

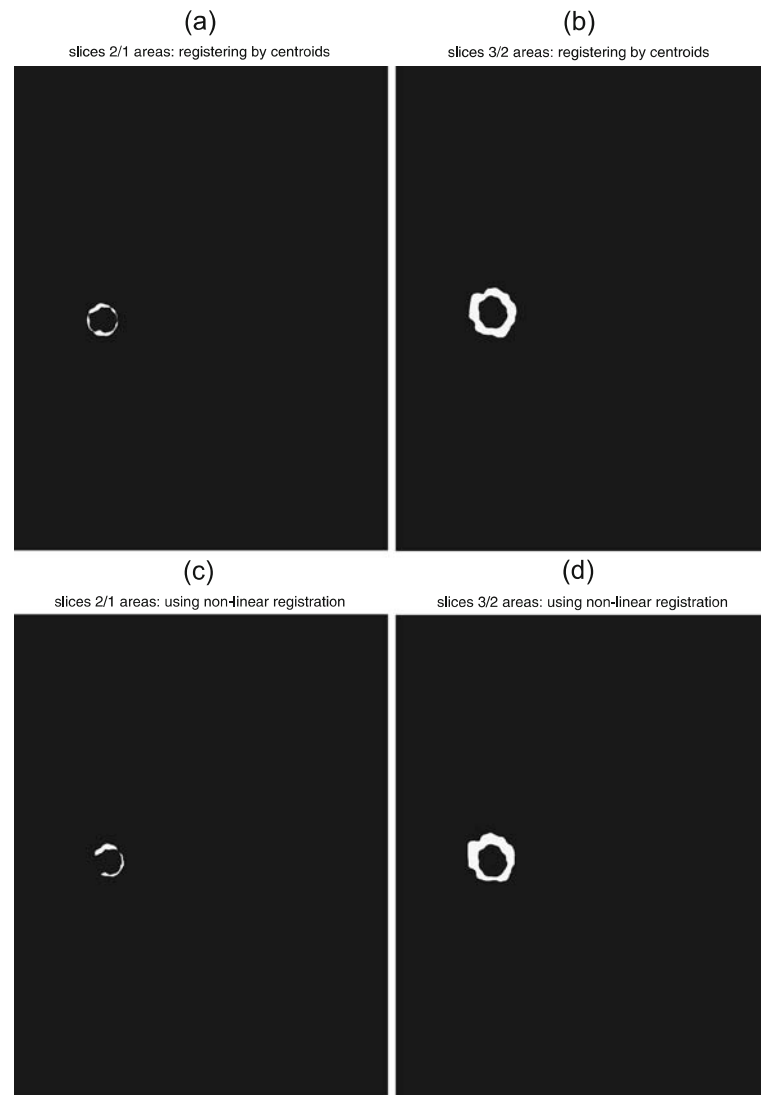slices 3/2 areas: using non-linear registration

Fig 9. Comparing tumor area growth in case 2 (based on the central slice), using linear transformations (a–b), and nonlinear transformations (c–d). Tumor areas registered using linear transformations (centroid adjustment): a area growth from April 09, 2007 to August 30, 2007; b area growth from August 30, 2007 to December 27, 2007; tumor areas registered using a typical nonlinear registration method (see Zhao et al.[8]): c area growth from April 09, 2007 to August 30, 2007; d area growth from August 30, 2007 to December 27, 2007.

tumor to treatments and the rate at which it decreases in size, and/or to create a growth pattern that can be compared to the evolution of the same type of tumor with similar treatment. The proposed model fits a given data set while minimizing the least squared error criterion (it is optimal, see "Modeling Unconstrained Tumor Growth"). The problem of fitting an exponential model is reduced

to fitting a linear model (see Eq. 13), and since the minimum number of data points to define a line is two, at least two data points are required to find the optimal model parameters in Eq. 22. Despite that more data points tend to produce even better results, it may not be practical to obtain many CT scans of the same patient in a short time span. We showed in our experimental results that only three

(a)

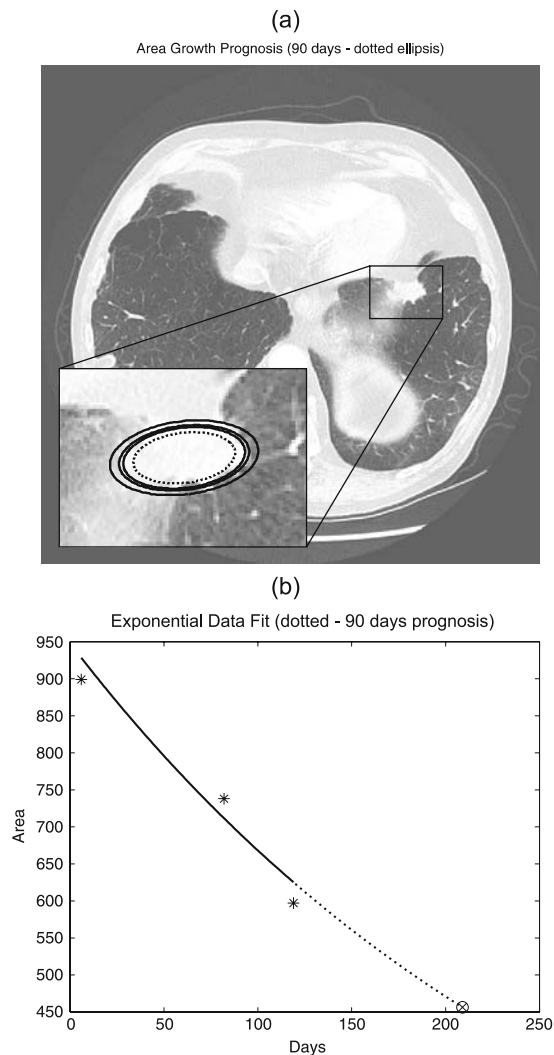Area Growth Prognosis (90 days - dotted ellipsis)

(b)

Fig 10. Measured tumor area shrinkage based on the central slice (case 3). Tumors are registered using linear transformations (centroid adjustment): a tumor shrinkage based on the different observations, approximated by *solid line ellipses*, and the 90 days prognosis obtained using the exponential model (*dotted line ellipsis*); b exponential model fit to the measured tumor areas (*solid line*), and the 90 days prognosis based on the tumor shrinkage rate obtained with the exponential model (*dotted line*).

data points have been sufficient to find the optimal model parameters, since these parameters produced an adequate model for available data.

CONCLUSIONS

The present work introduces a new method for assessing the growth of lung tumors quantitatively. An interactive tumor segmentation technique

based on active contours is used to recover the shape and size of a tumor. The segmentation method is efficient for locating the tumor margins, even if the tumor shape is irregular and contains concavities. The method presents good convergence and robustness to the initialization conditions and requires a simple and intuitive user interaction.

This approach can be used to evaluate the tumor growth rate without imposing shape constraints. The model presented potentially can be used to assess the tumor aggressiveness and the response of the tumor to treatments and to estimate a growth pattern. To estimate the growth pattern can be important for predicting the harmful potential to neighboring organs and anticipating more accurately the complications and maybe the need for more aggressive treatment orientation. Our focus is on the assessment of a potential invasion or rupture of adjacent vessels and extract trends as all tumors may not have the same pattern.

As a future work, we plan to evaluate the proposed technique in clinical trials and test its performance as a quantitative measure of tumor regression in response to treatment.

REFERENCES

1. Silva LS, Gaviao W, Koff D, Scharcanski J: Interactive tumor growth evaluation using adaptive image segmentation, Proceedings of the 2008 Annual Meeting of the Society for Imaging Informatics in Medicine (SIIM), May 15–18, Seattle, USA, 2008

2. Zacharaki EI, Hogea CS, Biros G, Davatzikos C: A comparative study of biomechanical simulators in deformable registration of brain tumor images. IEEE Trans Biomed Eng 55:1233–1236, 2008

3. Kyriacou SK, Davatzikos C, Zinreich SJ, Bryan N: Nonlinear elastic registration of brain images with tumor pathology using biomechanical model. IEEE Trans Med Imag 18(7):580–592, 1999

4. Clatz O, Sermesant M, Bondiau PY, Delingette H, Warfield SK, Malandain G, Ayache N: Realistic simulation of the 3-D growth of brain tumors in MR images coupling diffusion with biomechanical deformation. IEEE Trans Med Imag 24:1334–1346, 2005

5. Zacharaki EI, Matsopoulos GK, Nikita KS, Stamatakos GS: An application of multimodal image registration and fusion in a 3D tumor simulation model, Proceedings of the 25th. Int. Conf. of the IEEE EMBS, 2003

6. Armato SG, Oxnard GR, Kocherginsky M, Vogelzang NJ, Kindler HL, MacMahon H: Evaluation of semiautomated measurements of mesothelioma tumor thickness on CT scans. Acad Radiol 12:1301–1309, 2005

7. Zhao B, Schwartz LH, Moskowitz CS, Ginsberg MS, Rizvi NA, Kris MG: Lung cancer: Computerized quantification of tumor response—initial results. Radiology 241:892–898, 2006

8. Zhao B, Schwartz LH, Moskowitz CS, Ginsberg MS, Rizvi NA, Kris MG: Tracking tumor growth rates in patients with malignant gliomas: A test of two algorithms. Am J Neuroradiol 22:73–82, 2001

9. Xu C, Prince JL: Gradient vector flow: A new external force for snakes, Proc. of the IEEE Int. Conf. Computer Vision and Pattern Recognition, pp. 66–71, 1997

10. Kass M, Witkin AP, Terzopoulos D: Snakes: Active contour models. Int J Comput Vis (1) 4:321–331, 1988

11. Prince JL, Davatzikos C: Convexity analysis of active contour algorithms. Image Vis Comput 17(1):27–36, 1999

12. Jain AK: Fundamentals of digital image processing, Englewood-Cliffs: Prentice Hall, 1989

13. Dwight F: Mix random signal processing, Englewood-Cliffs: Prentice Hall, 1995, pp. 285–286

14. Suzuki C, Jacobsson H, Hantschek T, Torkzad M, Boden K, Eriksson Y, Berg E, Fujii H, Kubo A, Blomquist L: Radiologic measurements of tumor response to treatment: Practical approaches and limitations. RagioGraphics 25(2):329–344, 2008

15. Wong A, Bishop W: Efficient least squares fusion of MRI and CT images using a phase congruency model. Pattern Recogn Lett 29(3):173–180, 2008